Crystal structures and Conductivity properties of $MBi_6V_2O_{15}$ family type compounds (M=Pb, Sr, Ca, Cd, $Na_{0.5}Bi_{0.5}$)

Olfa Labidi, Michel Drache*, Pascal Roussel and Jean-Pierre Wignacourt

Unité de Catalyse et de Chimie du Solide - CNRS UMR 8181,
Equipe de Chimie du Solide ; ENSC et UST Lille ;
BP 90108 - 59652 Villeneuve d'Ascq Cedex, France

Suggested running head: $M$$Bi_6V_2O_{15}$-Family type ($M$=Pb, Sr, Ca, Cd, $Na_{0.5}Bi_{0.5}$)

Suggested figure for Graphical abstract: Fig.0

(*), to whom correspondence should be addressed,

Unité de Catalyse et de Chimie du Solide - CNRS UMR 8181,
Equipe de Chimie du Solide ; ENSC et UST Lille ;

BP 90108 - 59652 Villeneuve d'Ascq Cedex, France

Telephone: (33)320436587. Fax: (33)320436814

e-mail: michel.drache@ensc-lille.fr

Abstract: A family of compounds was prepared as powder samples with nominal formulas MBi$_6$V$_2$O$_{15}$ (M=Pb, Sr, Ca, Cd, Na$_{0.5}$Bi$_{0.5}$), as well as single crystals with closely related compositions. Single crystal structure determinations were realized using X-ray diffraction. Each sample crystallizes in a monoclinic cell related to the δ-Bi$_2$O$_3$ fluorite type cell, through the relationship: $\vec{a}_{m.}=3/2\,\vec{a}_F + 3/2\,\vec{b}_F + 3\,\vec{c}_F$, $\vec{b}_m= 3/2\,\vec{a}_F - 3/2\,\vec{b}_F$, $\vec{c}_m= 2\,\vec{a}_F + 2\,\vec{b}_F - 4\,\vec{c}_F$. With M=Na$_{0.5}Bi_{0.5}$, the non-centrosymetric C2 space group was selected, while for M=Pb-Cd, the structures were determined in the centrosymetric space group C2/c. Whatever the M element, a non-stoichiometric phase can be obtained. For M= Sr, Ca and Cd, mixed sites were observed; from their refined M/Bi occupancy factors, a determination method of Pb/Bi ratios has been proposed. These phases adopt a layer like structural model related to the δ-Bi$_2$O$_3$ fluorite structure, built from stacking slab units of cationic triple layers [(Bi, V) / (Bi, Bi/M) / (Bi, V)] where the vanadium atoms are located in the two external layers. Oxygen atoms are trapped either in cationic tetrahedrons (OBi$_4$, O(Bi/M)$_4$) for those within the slabs, or in VO$_4$ vanadates for those in the inter-slab spaces, thus limiting the materials oxide conductivity.

Key words

- alkaline-earth bismuth vanadium based mixed oxide.
- lead bismuth vanadium based mixed oxide.
- cadmium bismuth vanadium based mixed oxide.
- sodium bismuth vanadium based mixed oxide
- single crystal structure refinement.
- electrical conductivity properties
- structure-conductivity properties correlation

1. Introduction

The δ-Bi_2O_3 variety, which crystallizes in a fluorite-type structure, is known to date to be the best oxide anion conducting material at high temperature; for a review, see [1]. This interesting conductivity property [2] has been attributed to the defective and disordered characters of the oxide sub-lattice, associated to the high polarizability of Bi^{3+} cations [3]. With the aim of obtaining structurally related phases, keeping the interestingly high conducting properties, or reaching even better ones at temperatures as low as possible, numerous investigations of bismuth rich domains in binary systems [4-14], ternary systems [15] or quaternary ones [16] were carried out. Many δ-related phases could be stabilized at room temperature. Their conductivity performances are unfortunately poorer than that of the high temperature δ-Bi_2O_3 variety, due to the ordering of the oxygen network. The oxide mobility appears to be linked to the polarizability of cationic sub-network; the higher the bismuth content, the higher is the materials conductivity.

The ternary systems PbO-Bi_2O_3-P_2O_5/As_2O_5/V_2O_5 are among the most investigated systems; the existence of $PbBi_6X_2O_{15}$ (X=V, P, As) was established by Jie [17]. For $PbBi_6V_2O_{15}$, he identified an orthorhombic cell with *a*=11.970Å, *b*=11.023Å, *c*=17.324Å. Lee [18], proposed another unit cell from indexing the powder X-ray data, i.e.: *a*= 23.983(18) Å, *b*=17.172(13) Å, *c*=11.092(11) Å. Hitherto, to our knowledge, the structure has not been solved. The various authors agree that this compound derives structurally from the fluorite-type cubic form of δ-Bi_2O_3. Complete P or As for V substitutions in $PbBi_6V_2O_{15}$ produce solid solutions: $PbBi_6V_{2-x}P_xO_{15}$ and $PbBi_6V_{2-x}As_xO_{15}$ [18, 19]. On the other hand, two domains of limited solid solutions $PbBi_6P_{2-x}As_xO_{15}$ are obtained with a two-phase area for x compositions ranging between 0.30 and 1.55; another solid solution $Pb_{1-x}Sr_xBi_6V_2O_{15}$ is also observed. Lee concludes that the materials $PbBi_6X_2O_{15}$ (X=V, P, As) and $SrBi_6V_2O_{15}$ are isomorphous. The conductivities measured on these materials decrease in the order: $SrBi_6V_2O_{15}$ > $PbBi_6V_2O_{15}$ > $PbBi_6As_2O_{15}$ > $PbBi_6P_2O_{15}$ [18].

New investigations, reported in this paper, were realized with the aim of basically determining the crystal structures of several members of this family, then correlating the structures to the fluorite-type δ- Bi_2O_3, as well as the structural modifications to the evolution of the conductivity performances.

2. Experimental.

2.1. Syntheses.

Powder samples of MBi$_6$V$_2$O$_{15}$ (M=Pb, Sr, Ca, Cd, Na$_{0.5}$Bi$_{0.5}$) were prepared by solid state reaction of stoechiometric amounts of the starting reagents: Bi_2O_3 (Aldrich, 99.9%) and V_2O_5 (Aldrich, 99.6%), while introduction of the appropriate "divalent cation" was realized using PbO (Riedel de Haën, 99%), CdO, strontium or calcium carbonate, and a mixture of Na_2CO_3 and Bi_2O_3 in Na/Bi equimolar proportions. Reagents were weighed, mixed in an agate mortar and then fired at temperatures between 600°C and 800°C for a week, with intermediate regrindings in order to obtain the desired phase.

Single crystals were obtained from powder sample melting at 1000°C, followed by slow cooling at 1°C/h until 840°C, and then furnace disconnection. The selection of good quality crystals was based upon the sharpness of the observed diffraction spots.

2.2. Characterizations

Polycrystalline samples were investigated using various techniques. X-ray powder diffraction data were collected at room temperature using a D8 Advance Bruker. The pattern reflections were indexed from the crystalline cell identified on single crystals. The high temperature X-ray diffraction diagrams were explored using a Guinier-Lenné diffraction system with Cu$K\alpha$1 radiation to investigate whether any phase transitions exist; these observations were corroborated by thermal studies (differential thermal analysis DTA) performed on a Linseis L62 instrument. For investigation of electrical properties, sintered pellets (diameter and thickness around 5 mm) were elaborated from materials sintering at 850°C for 48h. The relative density of the sintered samples was nearly 85%. Gold electrodes were then sputtered on both flat faces of the pellets and measurements were done by impedance spectrometry in the range 1-10^6 Hz using a Schlumberger 1170 frequency response analyzer. Each set of values was recorded after 1 h stabilization stage.

None of the thermal studies indicated a phase transformation between the sintering temperature and the ambient one. A structural characterization on single crystal using the Bruker X8 CCD 4K diffractometer was realized for each composition at room temperature.

3. Structural Investigation

Single crystals were obtained from the melts of various nominal compositions MBi$_6$V$_2$O$_{15}$ (M=Pb, Sr, Cd, Ca, Na$_{0.5}$Bi$_{0.5}$), generally in the form of rectangular plates; in each case, a crystal was selected for the collection of the diffracted intensities. The SAINT 7.12 Software [20] was used to extract reflection intensities from the collected frames and the SADABS 2006/1 program [21] was used to correct data from absorption effects using a semi-empirical method based on redundancy. The crystal structures were solved by direct methods using the software SIR97 [22] which readily established the heavy atoms positions (Pb, Bi, V). Oxygen atoms were localized from difference Fourier maps. The last cycles of refinement included atomic positions, anisotropic displacement parameters for all non-oxygen atoms, and isotropic displacement parameters for oxygen atoms. Full-matrix least squares structure refinements against F were carried out using JANA2000 [23]. In the structural refinement procedure, VO_4 tetrahedrons were treated as rigid "molecular" groups. The rigidity of the molecule was determined by a number of common parameters for all atoms of the molecule. Each position of the molecular model was defined by 3 rotations (Φ, χ, ψ) and 3 translations (xtrans, ytrans, ztrans). The main results of the refinement stages are regrouped in Table I.

Hereafter, as an example, the structural resolution is presented for the calcium based sample, particularly representative in the series Pb-Ca. An orthorhombic F cell was initially identified with the parameters: a=11.546(2)Å, b=19.934(4)Å, c=52.231(2)Å. The high Rint=0.637 value highlighted a possible error on symmetry. The structure fits in fact in a monoclinic C cell: a=19.7711(6) Å, b=11.5481(3) Å, c=27.6881(8) Å, β=110.773(4)° (Rint=0.0830 after absorption correction). The most intense reflections characterize a sub-cell of the standard mother structure: a fluorite δ-Bi$_2$O$_3$. The matrix relationship between this monoclinic cell and the cubic δ fluorite-type cell is:

$$\begin{pmatrix} a \\ b \\ c \end{pmatrix} = \begin{pmatrix} 3/2 & 3/2 & 3 \\ 3/2 & -3/2 & 0 \\ 2 & 2 & -4 \end{pmatrix} \begin{pmatrix} a \\ b \\ c \end{pmatrix}_{\delta}$$

Taking into account the systematic extinctions, the space group is either C$2/c$ or Cc. The centrosymmetrical space group C$2/c$ was retained after refinement. The 144 heavy atoms within the unit cell are distributed as 14 general positions for bismuth and 4 general positions for vanadium (Fig. 1-a). The Bi11, Bi12, Bi13 and Bi14 sites are partially occupied by calcium and bismuth. Vanadium atoms were regarded in their close oxygen environment as

VO_4 tetrahedral rigid groups and refined as such (Fig. 1-b). In the case of the calcium based sample two tetrahedral configurations $V(1d)O_4$ and $V(1e)O_4$ are identified, indicating an oxygen disorder (Fig. 2). The atomic coordinates and isotropic/equivalent* parameters are given in Table II, and the atomic displacement parameters are regrouped in Table III.

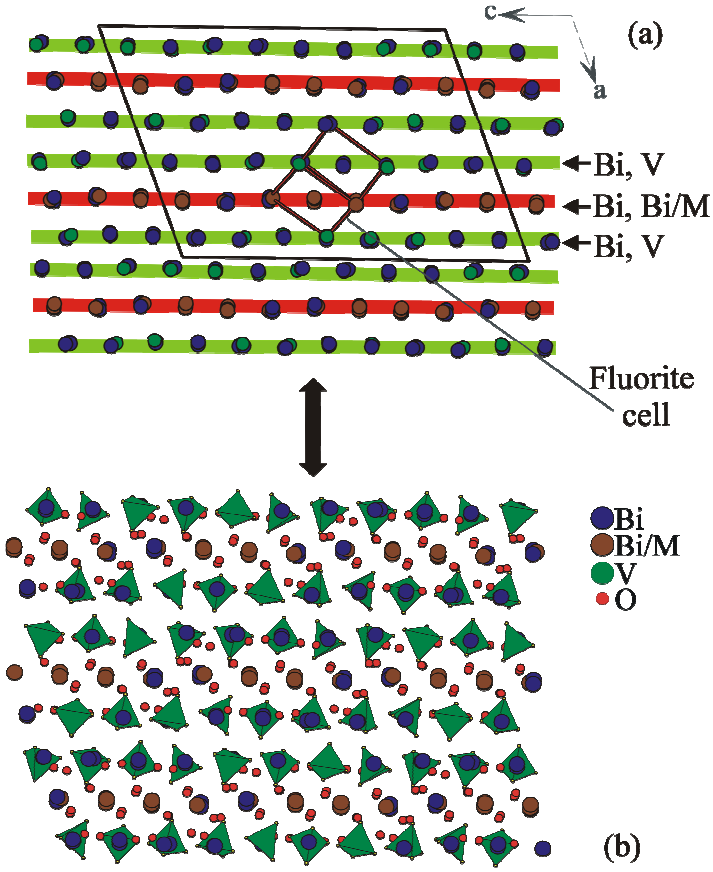

Figure 1: (010) projection of MBi$_6$V$_2$O$_{15}$ related structures (M=Pb, Sr, Ca, Cd, Na$_{0.5}$Bi$_{0.5}$): Ca based sample. Viewing of related fluorite cell (a), and VO_4 tetrahedrons (b).

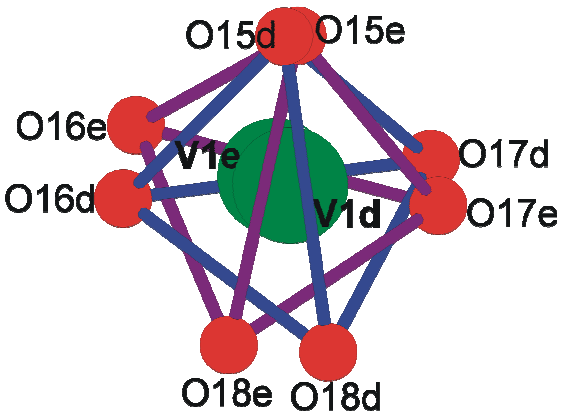

Figure 2: disordered VO_4 in Ca based MBi$_6$V$_2$O$_{15}$ related sample.

Structural refinements on single crystal led to a non-stoichiometric formulation $[Ca_{1.966(3)}Bi_{12.034(3)}]V_4O_{30}$, characteristic of a sample belonging to a solid solution. Three similar homologous phosphates ($Bi_6TP_2O_{15+x} \equiv T_2Bi_{12}P_4O_{30+2x}$) were recently reported [24]. In each of these, the non-stoichiometry was proposed from the existence of mixed cationic sites, and also a partially occupied oxygen site. For the three reported samples (T=Fe, Ni, Zn) the oxygen content has been evaluated from the occupancy refinement of the related oxide site, which was in agreement with the calculated formula using the usual oxidation number of the non oxygen elements. In our work, the structural investigation did not permitted identification of any supplementary oxygen site in agreement with the Bi^{3+} for Ca^{2+} substitution in $Ca_2Bi_{12}V_4O_{30}$ identified from the refinement. However, in the Ca based sample, taking into account the usual oxidation states of the (Ca^{2+}, Bi^{3+}, V^{5+}) cations, the neutral formulation of the sample would be $[Ca_{1.966(3)}Bi_{12.034(3)}]V_4O_{30.017}$.

The structural resolution was similar for related materials containing lead, strontium or cadmium, but was somewhat different for the Na containing material, which was refined in a C2 non-centrosymmetrical space group (i.e. determination of 36 heavy atom positions). In the case of strontium, cadmium or Na containing sample, the non-stoichiometric formulation was unambiguously identified from the structural resolution; the corresponding charge balanced formulas are respectively $[Sr_{1.43(4)}Bi_{12.57(4)}]V_4O_{30.285}$, $[Cd_{1.838(5)}Bi_{12.162(5)}]V_4O_{30.081}$, $[Na_{0.834(3)}Bi_{13.166(3)}]V_4O_{30.166}$.

A similar oxygen environment around the Bi, Sr, Cd or Ca cations, characterized by 3 types of polyhedron, with a coordinence ranging from 6 (distorted octahedron) to 8 (distorted cube), is observed for the various samples. The effect of the $6s^2$ lone pair is clearly enlighted by the distorted geometry of these polyhedrons. The structures of $MBi_6V_2O_{15}$ (*M*=Pb, Sr, Cd, Ca, $Na_{0.5}Bi_{0.5}$) family compounds can be described either by the stacking of 6 cationic layers along the *a* axis (Fig. 1-a), or 8 cationic layers along the *c* axis. Note that the *M* atoms are only located in one out of three cationic layers parallel to the (100) crystallographic plane.

Hitherto, $PbBi_6V_2O_{15}$ and $SrBi_6V_2O_{15}$ seemed to correspond to definite compounds [19]. The structural determinations carried out in this work on the $MBi_6V_2O_{15}$ type family (*M*=Sr, Cd, Ca, $Na_{0.5}Bi_{0.5}$), evidence several mixed *M*-Bi sites, showing the existence of solid solutions domains. For *M* = Sr, Cd and Ca, the refinements have been realized in the C2/c space group; in the case of "$PbBi_6V_2O_{15}$" refinement, which has been conducted in the same space group, the existence of similar mixed sites can be presumed. From the experimental data reported in Table I, and using the Shannon and Prewitt tables [25, 26], we have calculated the "mean radius" (VI coordinence) of the "mixed cationic species" present in sites

11, 12, 13 and 14, which are mixed sites in the Sr, Cd and Ca-samples. For these sites, this "radius" exhibits a quasi-linear dependence versus the unit cell volume. Each curve is calculated from a least square regression method, and a good R^2 correlation factor: 0.849(1), 0.906(1), 0.990(1) and 0.999(1) respectively for sites 11, 12, 13 or 14 (Fig. 3) is observed.

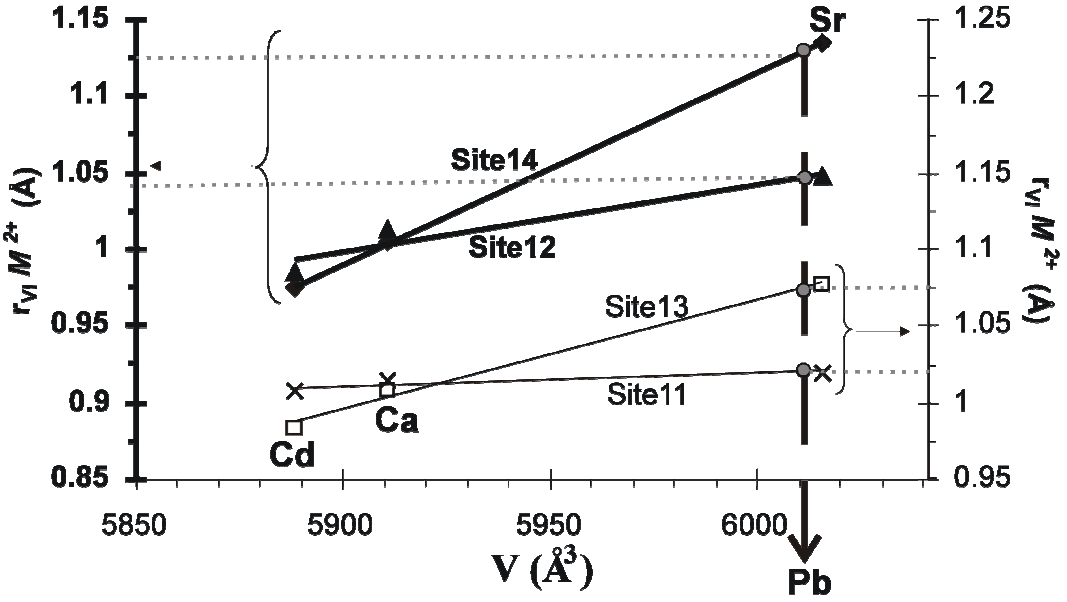

Figure 3. Dependence of the "mean cationic radius" versus Unit Cell volume, in the (Bi, *M*) mixed sites 11, 12, 13, 14 for MBi$_6$V$_2$O$_{15}$-type family.

Using these calibration graphs, the "mean" cationic radius in each "$PbBi_6V_2O_{15}$" corresponding site has been estimated from the cell volume. It leads to $\bar{r}_{VI}$≈1.019, 1.048, 1.075, 1.132Å for sites 11, 12, 13 and 14 respectively. The occupancy ratios of Bi^{3+} and Pb^{2+}, within each site, have thus been deduced using the values given in the Shannon and Prewitt table ($r_{VI}(Pb^{2+})$=1.18 Å and $r_{VI}(Bi^{3+})$=1.02 Å). It can then be proposed that site 11 is only occupied by bismuth, whereas the three other sites are Pb/Bi mixed sites. The Pb/Bi occupancy ratios determined from the cationic radii in the mixed sites and from the Pb^{2+} and Bi^{3+} radii are 0.175/0.825, 0.343/0.657 and 0.703/0.297, respectively for site 12, site 13 and site 14. Therefore, the charge balanced formula corresponding to the refined structure can be written: $Pb_{(0.175+0.343+0.703)}Bi_{(10+1+0.825+0.657+0.297)}V_4O_{30.391} \equiv Pb_{1.218}Bi_{12.782}V_4O_{30.391}$. It is worth to note that the occupancy of site 11, only by bismuth, is also observed in the case of the Sr based sample, likely due to the chemical similarity of Pb^{2+} and Sr^{2+} cations.

However, these values have to be considered carefully, keeping in mind that, in fluorite related structures, cations have a cubic anionic environment of eight sites, which are statistically occupied by six oxygen atoms. Then using the ionic radius values in coordinence eight, instead of six, leads to slightly different Pb/Bi occupancy ratios and to a somewhat different formula: site 11 is still only occupied by bismuth atoms, however the decrease of the bismuth/lead ratio from site 12 to site 14 is no longer monotonous, as observed for the Pb sample (using r_{VI} values), and for Sr, Cd or Ca samples.

The experimental powder X-ray patterns of the four MBi$_6$V$_2$O$_{15}$ materials correspond to the theoretical patterns calculated from the results of the structure determinations. For Sr based material which exhibits the largest discrepancy between the nominal composition and the composition refined from the single crystal X-ray data, we have realized a complete indexing of the powder X-ray pattern for the nominal composition SrBi$_6$V$_2$O$_{15}$. The refined cell parameters are: a=19.8466(7)Å, b=11.6092(4)Å, c=27.843(1)Å, β=110.645(2)°. The parameters evolution versus the composition variation of the solid solution is then very slight.

4. Conductivity properties.

Conductivity measurements were carried out on ceramic pellets of nominal compositions MBi$_6$V$_2$O$_{15}$, and the temperature dependence of the conductivity was evidenced from Arrhenius plots log (σT) = f (1/T). Representation of the 1st cooling (800-300°C) and of 2nd heating (300-850°C) runs overlap, and only the 2nd heating runs are presented for clarity of the figure. Table II regroups the significant values of this study at 500°C (conductivity: σ, and activation energy: Ea) and 800°C (σ). The conducting properties of the lead or strontium containing samples are similar to those obtained by Lee [18].

The Arrhenius plots underline some features: only the Sr containing material exhibits a linear domain over the whole investigated temperature range. Each of the other samples, less conducting, displays a curved domain of evolution. This is a typical behaviour of ionic solid conductors, in which the number of charge carriers, rather low at room temperature, increases significantly with the temperature. While preponderant oxide ion mobility can be reasonably presumed for Pb, Sr, Ca and Cd based materials, in the case of the Na based family member, a Na^+ cationic conductivity contribution cannot be excluded, and could even become preponderant. The specific high temperature behaviour of Na based sample, with the rapid

increase of σ versus temperature in the range 775-850°C, also shows that this sample cannot be considered with the other materials for the comparison of conductivity performances.

Over the whole investigated range, at a given temperature, the conductivity level decrease in the order Sr, Cd, Pb and Ca (Fig. 4). $SrBi_6V_2O_{15}$ sample, presents the weakest energy of activation, clearly distinct from the three other samples at low temperature (Table IV): at 300°C, the Sr based sample is nearly 10 times more conductive than all other samples.

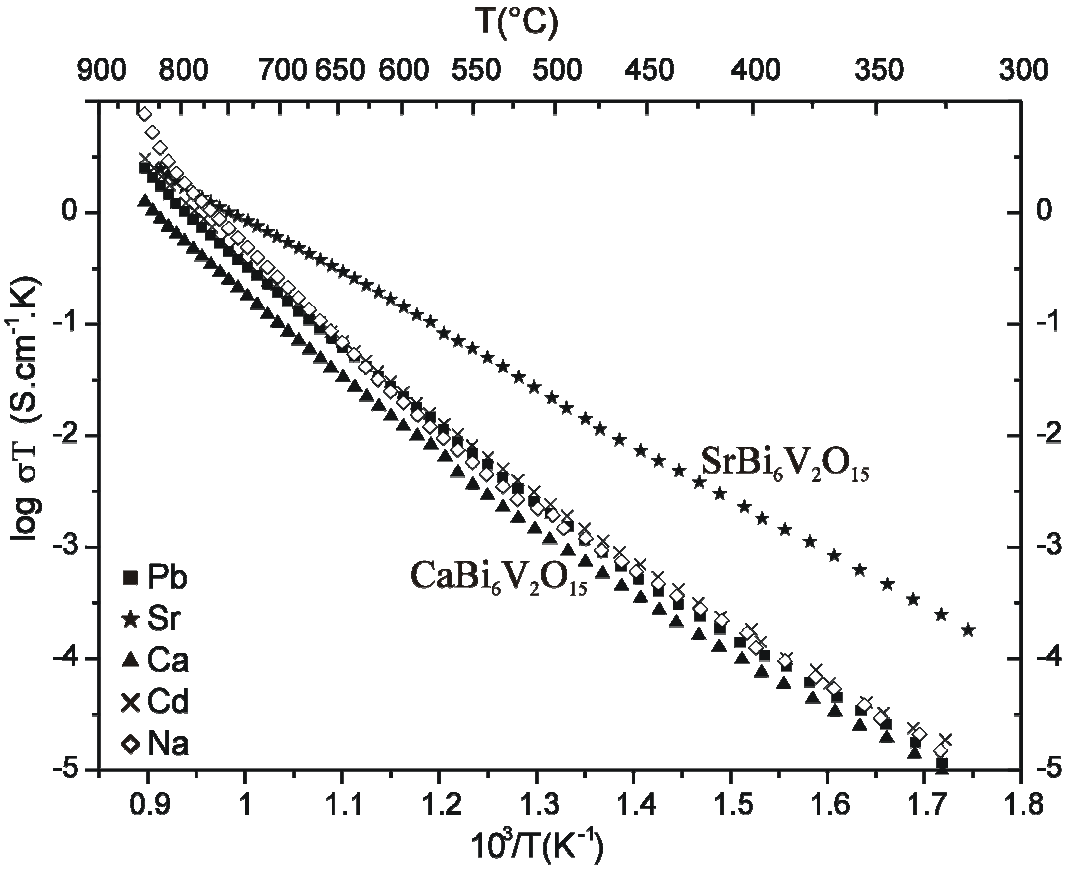

Figure 4: Conductivity Arrhenius plots of *M*$Bi_6V_2O_{15}$ materials (M=Pb, Sr, Ca, Cd, $Na_{0.5}Bi_{0.5}$).

5. Discussion and conclusion.

The fluorite type structures reported in this paper display a cationic organization of layer triplets, in which vanadium with its close oxygen environment is considered as VO_4 tetrahedrons, and can be distinguished as systematically located in the outer cationic layers, (Fig. 5-a). These triplets will be hereafter labelled “slabs”. Averaged distances between cationic layers are higher in inter-slab spaces (≈3.20-3.21 Å) than within the slabs (≈3.02-3.06

Å); for this later case, no evident correlation with the alkaline-earth cation size can be observed.

Another possible structural representation consists in considering OBi_4 and $O(Bi,M)_4$ anti-tetrahedral units (*M*=Pb, Sr, Ca, Cd, $Na_{0.5}Bi_{0.5}$) and VO_4 tetrahedral ones. It is so possible to identify cationic slabs made up of three "layers": [(OBi_4, $O(Bi/M)_4$, VO_4); (OBi_4, $O(Bi/M)_4$); (OBi_4, $O(Bi/M)_4$, VO_4)] in the various samples (Fig. 5-b). Thus, no supplementary oxygen atom is observed in the inter-slab space. This stacking design, similar to that considered in $Bi_{14}P_4O_{31}$ [$Bi_{12}P_6O_{33}$, $Bi_{18}O_{27}$] or in $Bi_{50}V_4O_{85}$ [27], can be used also in $Bi_{46}X_8O_{89}$ (X=P, V) [28] or $Pb_5Bi_{18}P_4O_{42}$ [29].

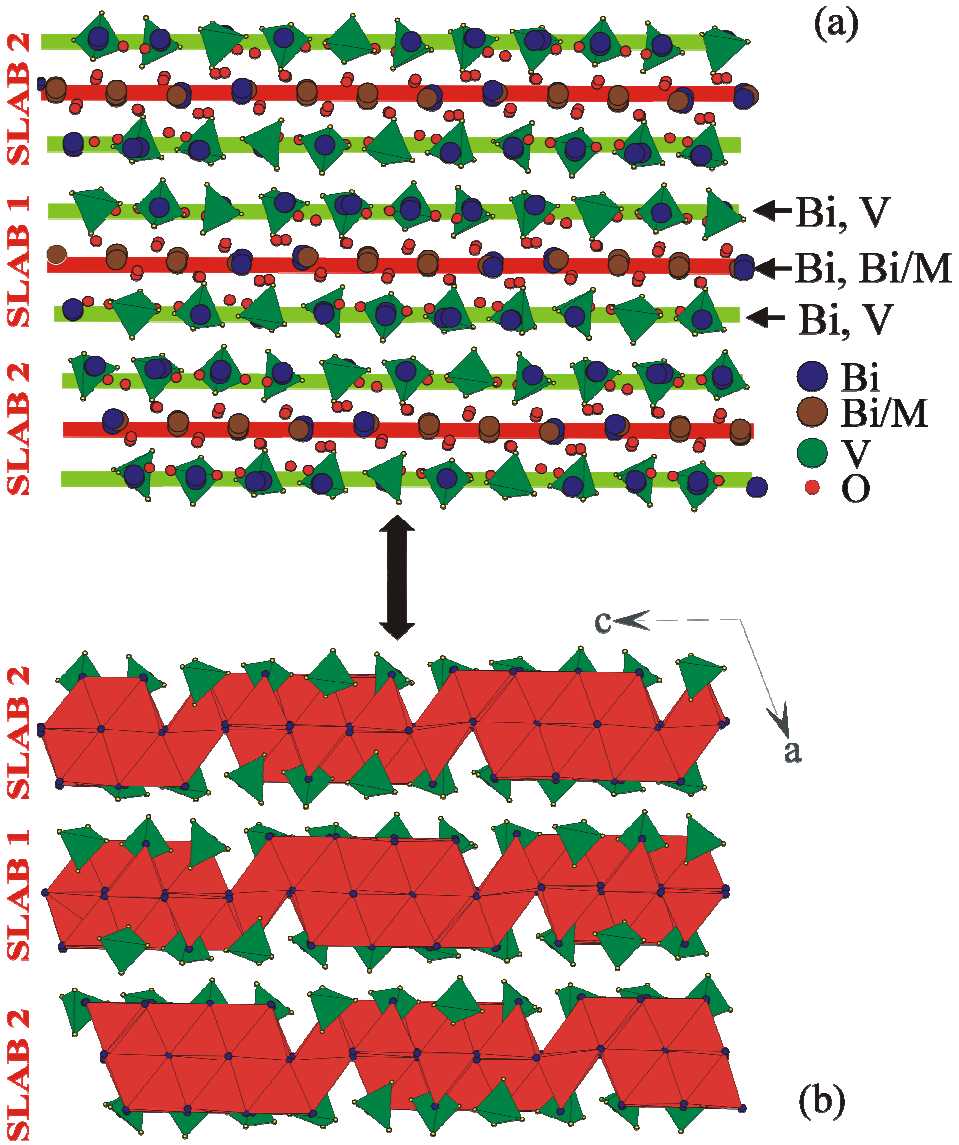

Figure 5: *M*$Bi_6V_2O_{15}$ related structure (*M*=Pb, Sr, Cd, Ca, $Na_{0.5}Bi_{0.5}$) viewed as cationic layers *(a)* or OBi_4, $O(Bi, M)_4$ and VO_4 tetrahedron layers arrangements *(b)*.

The slab organization is related to the important oxygen environment in the vicinity of external layers of the slabs. The oxygen content of the external layers and the inter-slab distance are correlated, as shown by the slight expansion of inter-slab space observed from $Bi_{50}V_4O_{85}$ (≈3.30 Å) to $Bi_{46}V_8O_{89}$ (≈3.36 Å), whereas distances between cationic layers within the slabs do not vary (≈3.16 Å). Resulting from the decrease of the averaged cationic radius, when 4 vanadium atoms substitute for 4 bismuth atoms, a contraction of the layers would appear. In fact, this negligible influence is destroyed by an increase of the oxygen atoms number, which leads to a dilatation of inter-slab spaces.

The described slabs are built out of cationic planes corresponding to (111) planes of a standard fluorite cubic cell which was crushed along the [111] direction. Going from the fluorite lattice to the considered structure, leads to a decrease of the interlayer distances; the shortest distances (2/3) correspond to the interlayer distances within the slabs, and the longer ones (1/3) to the interslabs. This shrinkage along the [111] direction, compared to the fluorite cubic lattice, is also observed for the slab structures of the rhombohedral type, based either on alkaline-earth or rare earth [1]. The comparison of one inter-slab plus one slab thickness, to the [111] diagonal of an ideal cubic lattice calculated for the same cell volume (Fig. 6) makes possible to evaluate the shrinkage of the fluorite lattice in our samples. It thus seems that an intermediary M^{2+} size (Sr) yields a structure with a maximal crushing of the fluorite lattice.

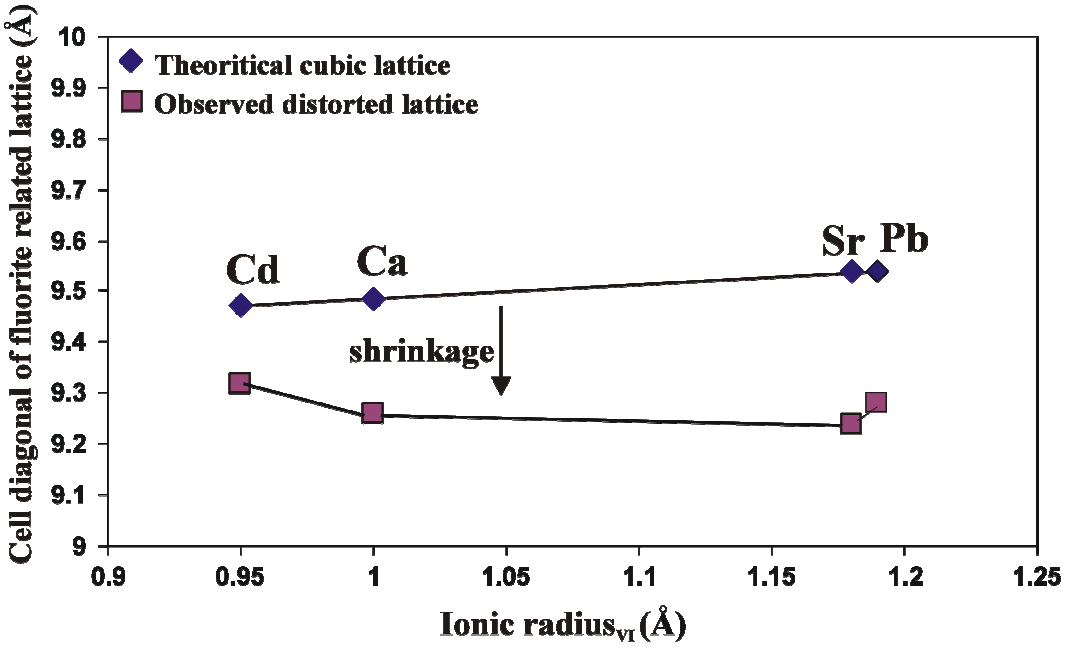

Figure 6: MBi$_6$V$_2$O$_{15}$–type materials (M=Pb, Sr, Ca, Cd): Evolution of « slab+interslab » thickness (observed distorted lattice), and of theoretical cubic fluorite cell diagonal, versus r_{VI} (M^{2+}).

According to Lee [18], $PbBi_6V_2O_{15}$ and $SrBi_6V_2O_{15}$ conductivities do not show any evolution, when the atmosphere evolutes from air (PO_2≈0.2atm) to nitrogen; the electronic contribution to conductivity is negligible. Consequently these materials can be considered as pure ionic conductors. On the basis of the slab model in rhombohedral Bi-Sr-O type phases, the conductivity of $MBi_6V_2O_{15}$–type materials might result from oxide ions moving into the inter-slab spaces. The oxygen evidenced in these spaces is trapped in VO_4 tetrahedrons. In each cationic layer (central or lateral/external layer of the slab), the crushing of the fluorite structure led to a spacing of the cations compared to their relative location in the cubic lattice. The higher the crushing, the higher is the possibility for the oxygen atoms to move, between the cations, from inside the slabs towards the inter-slab spaces, and consequently, the higher is the oxide conductivity. This is in good agreement with the best conductivity performance noted for the Sr based material.

The cationic model of layer triplets [(Bi, V) / (Bi, Bi/*M*) / (Bi, V)] where the vanadium atoms are placed in the external layers, is well adapted to the compounds highlighted in this work, but fits also with the other vanadates / phosphates fluorite type structures reported in the literature: $Bi_{50}V_4O_{85}$, $Bi_{46}X_8O_{89}$ (*X*=V, P), $Pb_5Bi_{18}P_4O_{42}$, $Bi_{14}P_4O_{31}$ [27-29]. The limited conductivity of the $MBi_6V_2O_{15}$–type materials is likely related to the trapping of the oxygen atoms of the inter-slabs space in VO_4 tetrahedral units.

5. Supplementary material.

Crystal Structure Data for the various phases gathered in Table I, have been sent to the Fachinformationzentrum Karlsruhe, 76344 Eggenstein-Leopoldshafen, Germany (fax: (+49)7247-808-666; e-mail: crystaldata@fiz-karlsruhe.de; http://www.fiz-karlsruhe.de/ecid/Internet/en/icsd/depot_anforderung.html), as supplementary material CSD Nos. 391414 ($PbBi_6V_2O_{15}$), 391415 ($SrBi_6V_2O_{15}$), 391416 ($CaBi_6V_2O_{15}$), 391417 ($CdBi_6V_2O_{15}$), 391418 ($Na_{0.5}Bi_{6.5}V_2O_{15}$). Copies of this information can be obtained by contacting the FIZ (quoting the article details and the corresponding CSD number).

References:

[1] Drache M., Roussel P., Wignacourt J. P., Chem. Rev., 107 (2007) 80.

[2] Takahashi T., Iwahara H., Nagai Y., J. Appl. Electrochem. 2 (1972) 97.

[3] Harwig H. A., Zeitschrift für Anorganishe und Allgemeine Chemie, 444 (1978) 151.

[4] Takahashi T., Iwahara H., Arao T., J. Appl. Electrochem., 5 (1975) 187.

[5] Takahashi T., Esaka T., Iwahara H., J. Appl. Electrochem., 5 (1975) 197.

[6] Iwahara H., Esaka T., Sato T., Takahashi T., J. Appl. Electrochem., 39 (1981) 173.

[7] Verkerk M.J., Burgraaf A. J., Solid State Ionics, 3 / 4 (1981) 463.

[8] Watanabe A., Kikuchi T., Solid State Ionics, 21 (1986) 287.

[9] Conflant P., Follet-Houttemane C., Drache M., J. Mater. Chem., 1 (1991) 649.

[10] Takahashi T., Iwahara H., J. Appl. Electrochem., 3 (1973) 65.

[11] El Harrak A., Conflant P., Drache M., Boivin J. C., J. Chim. Phys., 88 (1991) 2281.

[12] Omari M., Drache M., Conflant P., Boivin J.C., Solid State Ionics, 40 / 41 (1990) 929.

[13] Meng G., Chen C., Han X., Yang P., Peng D., Solid State Ionics, 28 / 30 (1988) 533.

[14] Mercurio D., El Farissi M., Frit B., Réau J. M., Senegas J., Solid State Ionics, 39 (1990) 297.

[15] Portefaix N., Conflant P., Boivin J. C., Wignacourt J. P., Drache M., J. of Solid State Chem., 134 (1997) 219.

[16] Benkaddour M., Omari M., Boivin J. C., Conflant P. Drache M., Annales de Chimie Sc. des Mat., 25 (2000) S165.

[17] Jie Y. C., Eysel W., Powder Diffraction, 10-2 (1995) 76.

[18] Lee C. S., Lee C. K., Sinclair D. C., Zainal Z., Hashim M., Solid State Ionics : Trends in the new millennium, 553 (2002).

[19] Lee C. K., Lee C. S., Watanabe A., Sinclair D. C., Solid State Ionics, 171 (2004) 237.

[20] Bruker Analytical X-ray system, “SAINT+, Version 7.12”, Madison, USA, 2004.

[21] Sheldrick G. M., SADABS, Bruker-Siemens Area Detector Absorption and Other Correction, Version 2004/1, Goetingen, Germany (2004).

[22] Altomare A., Cascaro G., Giacovazzo C., Guagliardi A., Burla M. C., Polidori G., Camalli M., “SIR 97’’, J. Appl. Crystallogr., 27 (1994) 434.

[23] Petricek V., Dusek M. and Palatinus L., JANA2000, Institute of Physics, Praha, Czech Republic (2005).

[24] Arumugam N., Lynch V., Steinfink H., J. Solid State Chem., 2007, doi:10.1016/j.jssc.2007.02.018.

[25] Shannon R. D., Prewitt C. T., Acta Crystallogr., B26 (1970) 1046.

[26] Shannon R. D., Acta Crystallogr., A32 (1976) 751.

[27] Mauvy F., Launay J. C., Darriet J., J. Solid State Chem., 178 (2005) 2015.

[28] Darriet J., Launay J. C., Zuniga F. J., J. Solid State Chem., 178 (2005)1752.

[29] Giraud S., Wignacourt J.P., Swinnea S., Drache M., Steinfink H., Harlow R., J. Solid State Chem., 151 (2000) 181.

Table I: Crystal data and structure refinements for MBi$_6$V$_2$O$_{15}$ (M=Pb, Sr, Ca, Cd, Na$_{0.5}$Bi$_{0.5}$)

Nominal formula	$PbBi_6V_2O_{15}$ ≡ $Pb_2Bi_{12}V_4O_{30}$	$SrBi_6V_2O_{15}$ ≡ $Sr_2Bi_{12}V_4O_{30}$	$CdBi_6V_2O_{15}$ ≡ $Cd_2Bi_{12}V_4O_{30}$	$CaBi_6V_2O_{15}$ ≡ $Ca_2Bi_{12}V_4O_{30}$	$Na_{0.5}Bi_{6.5}V_2O_{15}$ ≡ $NaBi_{13}V_4O_{30}$
Refined formula	$Bi_{14}V_4O_{30}$	$[Sr_{1.43(4)}Bi_{12.57(4)}]V_4O_{30}$	$[Cd_{1.838(5)}Bi_{12.162(5)}]V_4O_{30}$	$[Ca_{1.966(3)}Bi_{12.034(3)}]V_4O_{30}$	$[Na_{0.834(3)}Bi_{13.166(3)}]V_4O_{30}$
Cell parameters (Å)	a=19.9345(3) b=11.5464(2) c=27.9515(4) β=110.8813(9)°	a=19.9112(9) b=11.5916(6) c=27.911(1) β=110.872(2)°	a=19.6969(6) b=11.5315(3) c=27.7679(8) β=110.993(1)°	a=19.7711(6) b=11.5481(3) c=27.6881(8) β=110.773(4)°	a=19.8603(5) b=11.5096(2) c=27.8321(5) β=111.172(3)°
Cell volume (Å^3)	6011.1(2)	6015.3(5)	5888.4(3)	5910.7(4)	5932.6
Crystal system	←		Monoclinic		→
Space group	←		C 2/c (N°15)	→	C 121(N°5)
Z	←		8		→
F000	11947	11432	11433	10957	11467
Intensity collection					
Wavelength (Å)	0.71073 (Mo$K\alpha$)	0.71073 (Mo$K\alpha$)	0.71073 (Mo$K\alpha$)	0.71073 (Mo$K\alpha$)	0.71073 (Mo$K\alpha$)
θ range (°)	1.56-36.63	1.56-39.39	1.57-37.93	1.57-40.32	1.57-37.52
Data collected	-27≤ h ≤33 -19≤ k ≤15 -46≤ l ≤42	-35≤ h ≤35 -19≤ k ≤20 -49≤ l ≤49	-34≤ h ≤34 -19≤ k ≤19 -32≤ l ≤46	-35≤ h ≤34 -20≤ k ≤21 -45≤ l ≤50	-33≤ h ≤33 -17≤ k ≤19 -47≤ l ≤47
No. of reflections collected	84100	71876	67175	90242	130120
No. of reflections measured	14872	17274	14509	18140	29862
No. of independent (I>3σ(I))	8681	10874	7543	10130	20787
Redundancy	5.655	4.161	4.63	4.975	4.357
Completeness / θ(°)	99.60% / 36.63°	96.44% / 39.39°	95% / 36.43°	97.91% / 40.32°	99.75% / 37.52°
μ_1 (Mo, Kα) mm^{-1}	88.500	81.991	79.953	77.892	84.421
Tmin /Tmax ratio	0.0717	0.2027	0.3017	0.0706	0.3650
$R(F^2)_{int}$ before absorption correction	0.2154	0.2227	0.1765	0.2884	0.1980
$R(F^2)_{int}$ after absorption correction	0.0749	0.0720	0.0573	0.0830	0.0685
Refinement					
No. of parameters	227	230	231	238	428
Weighting scheme			$1/\sigma^2$		
R(F) obs./all	0.0572 / 0.1125	0.0623 / 0.1090	0.0541 / 0.1267	0.0608 / 0.1268	0.0534 / 0.0890
wR(F) obs./all	0.0552 / 0.0601	0.0656 / 0.0700	0.0537 / 0.0583	0.0688 / 0.0741	0.0512 / 0.0547
ρmax, ρmin (e-/Å^3)	8.52 / -8.26	11.08 / -8.40	9.84 / -6.07	14.33 / -13.16	4.60 / -10.72
Extinction coefficient	0.027(1)	0.046(2)	0.0120(8)	0.020(1)	0.04998(3)

Table II: Atomic occupancy factors, coordinates and isotropic/equivalent* parameters (Å^2) for $CaBi_6V_2O_{15}$. **Somme of occupancies for Bi/Ca mixed sites or atoms of the VO_4 disordered tetrahedron was fixed to 1.

Atoms	Occ.	x	y	z	Ueq*/Uiso
Bi1	1	0.25104(2)	0.68636(4)	0.190912(17)	0.01539(13)*
Bi2	1	0.23046(3)	0.03790(5)	0.18434(2)	0.02743(18)*
Bi3	1	0.58097(2)	0.83374(4)	0.05134(2)	0.02117(15)*
Bi4	1	0.40434(2)	0.99040(4)	0.064020(16)	0.01435(12)*
Bi5	1	0.08697(2)	0.19455(5)	-0.06291(2)	0.02252(15)*
Bi6	1	0.09811(2)	0.31063(4)	-0.185964(16)	0.01591(13)*
Bi7	1	0.58059(2)	0.02089(4)	0.186134(16)	0.01392(12)*
Bi8	1	0.41055(2)	0.51736(4)	0.188537(18)	0.01759(13)*
Bi9	1	0.57536(2)	0.70077(4)	0.181704(17)	0.01336(12)*
Bi10	1	-0.08261(2)	0.01231(4)	0.435004(17)	0.01491(12)*
Bi11	0.717(2)**	0.23790(3)	0.84345(5)	0.05772(2)	0.01618(19)*
Ca11	0.283**	0.2379	0.8435	0.0577	0.01618(19)*
Bi12	0.695(2)**	0.25453(3)	0.48361(6)	0.06033(3)	0.0222(2)*
Ca12	0.305**	0.2545	0.4836	0.0603	0.0222(2)*
Bi13	0.412(3)**	0.24382(5)	0.35768(9)	0.17808(4)	0.0257(3)*
Ca13	0.588**	0.2438	0.3577	0.1781	0.0257(3)*
Bi14	0.210(3)**	0.24210(7)	0.16748(13)	0.05791(6)	0.0282(6)*
Ca14	0.790**	0.2421	0.1675	0.0579	0.0282(6)*
O1	1	0.2827(4)	0.1698(6)	0.1611(3)	0.0163(15)
O2	1	0.6125(4)	0.8608(7)	0.1641(3)	0.0167(15)
O3	1	0.2974(4)	0.5409(7)	0.1671(3)	0.0228(18)
O4	1	0.1140(4)	0.3529(7)	-0.1086(3)	0.0185(16)
O5	1	0.1999(4)	0.1668(6)	-0.0353(3)	0.0167(15)
O6	1	0.6091(4)	0.6643(7)	0.0282(3)	0.0167(15)
O7	1	0.6259(5)	0.6215(8)	0.1332(4)	0.034(2)
O8	1	0.6911(5)	0.6737(8)	0.2248(4)	0.029(2)
O9	1	0.6976(4)	0.8558(7)	0.0890(3)	0.0253(19)
O10	1	0.2879(4)	0.9879(7)	0.0277(3)	0.0240(18)
O11	1	0.6001(5)	0.8554(8)	-0.0211(4)	0.029(2)
O12	1	-0.1950(4)	-0.0186(7)	0.4090(3)	0.0230(17)
O13	1	0.1925(5)	0.5507(8)	0.2081(4)	0.031(2)
O14	1	0.1267(7)	0.1438(11)	-0.1589(5)	0.064(4)
Atoms of tetrahedral rigid molecule					
V1	1	0.08634(9)	0.85609(15)	0.19785(7)	0.0121(3)*
O15	1	0.0724(5)	0.9841(7)	0.2244(4)	0.071(2)
O16	1	0.1628(5)	0.7998(9)	0.2348(4)	0.093(3)
O17	1	0.0181(5)	0.7640(8)	0.1900(4)	0.083(2)
O18	1	0.0895(6)	0.8836(9)	0.1390(3)	0.076(2)

Molecular rigid groups

Positions	Φ	χ	ψ	xtrans	ytrans	ztrans
Tetra 1	0	0	0	0	0	0
Tetra 2	-24.3(4)	14.0(4)	113.0(4)	0.31793(9)	-0.20938(16)	-0.13718(7)
Tetra 3	150.8(4)	1.2(4)	1.5(4)	0.31233(9)	0.00689(15)	-0.00983(7)
Tetra 4	161.0(15)	63.6(7)	19.4(14)	0.5022(2)	-0.7043(4)	-0.13472(17)
Tetra 5	146(2)	40.9(19)	9(2)	0.4995(7)	-0.6865(13)	-0.1341(5)

Atomic coordinates :

	Atoms	Occ.	x	y	z	Ueq*/Uiso
	V1a	1	0.08634(9)	0.85609(15)	0.19784(7)	0.0121(3)*
	O15a	1	0.0727(6)	0.9841(7)	0.2244(4)	0.071(2)
Tetra 1	O16a	1	0.1630(5)	0.7998(10)	0.2349(4)	0.093(3)
	O17a	1	0.0183(5)	0.7640(8)	0.1900(4)	0.083(2)
	O18a	1	0.0897(6)	0.8836(9)	0.1390(3)	0.076(2)
	V1b	1	0.40406(9)	0.64671(16)	0.06065(6)	0.0121(3)*
	O15b	1	0.3900(7)	0.5601(8)	0.1065(3)	0.071(2)
Tetra 2	O16b	1	0.4082(7)	0.5656(8)	0.0135(4)	0.093(3)
	O17b	1	0.3390(7)	0.7460(8)	0.0387(4)	0.083(2)
	O18b	1	0.4830(6)	0.7176(8)	0.0879(4)	0.076(2)
	V1c	1	0.39846(9)	0.86298(15)	0.18800(6)	0.0121(3)*
	O15c	1	0.3994(7)	0.7308(8)	0.2165(4)	0.071(2)
Tetra 3	O16c	1	0.3810(7)	0.9634(10)	0.2234(4)	0.093(3)
	O17c	1	0.4768(6)	0.8893(9)	0.1801(4)	0.083(2)
	O18c	1	0.3333(7)	0.8617(10)	0.1290(3)	0.076(2)
	V1d	0.74(3)**	0.5883(2)	0.1515(4)	0.06311(17)	0.0121(3)*
	O15d	0.74**	0.5503(5)	0.0782(9)	0.1010(5)	0.071(2)
Tetra 4	O16d	0.74**	0.5358(5)	0.2595(10)	0.0350(5)	0.093(3)
	O17d	0.74**	0.6711(5)	0.1986(10)	0.0977(5)	0.083(2)
	O18d	0.74**	0.5961(6)	0.0599(9)	0.0180(5)	0.076(2)
	V1e	0.26**	0.5857(7)	0.1697(13)	0.0637(5)	0.0121(3)*
	O15e	0.26**	0.5587(9)	0.0836(15)	0.1040(7)	0.071(2)
Tetra 5	O16e	0.26**	0.5466(9)	0.2960(15)	0.0587(7)	0.093(3)
	O17e	0.26**	0.6754(8)	0.1839(15)	0.0851(7)	0.083(2)
	O18e	0.26**	0.5603(9)	0.1063(15)	0.0052(6)	0.076(2)

Table III: Atomic displacement parameters (Å^2) for $CaBi_6V_2O_{15}$

Atome	U_{11}	U_{22}	U_{33}	U_{12}	U_{13}	U_{23}
Bi1	0.01484(18)	0.01283(19)	0.01820(19)	-0.00112(15)	0.00550(15)	-0.00154(17)
Bi2	0.0291(3)	0.0221(3)	0.0373(3)	-0.0017(2)	0.0195(2)	0.0058(2)
Bi3	0.0152(2)	0.0270(3)	0.0245(2)	-0.00076(17)	0.01081(17)	-0.00499(20)
Bi4	0.01466(18)	0.0133(2)	0.01520(18)	0.00389(14)	0.00540(15)	0.00246(16)
Bi5	0.01435(19)	0.0190(2)	0.0310(3)	-0.00142(16)	0.00396(18)	-0.0059(2)
Bi6	0.01631(19)	0.0180(2)	0.01218(17)	-0.00235(16)	0.00356(14)	-0.00236(16)
Bi7	0.01596(18)	0.01161(18)	0.01610(18)	0.00135(14)	0.00802(15)	-0.00021(15)
Bi8	0.01331(18)	0.0142(2)	0.0210(2)	-0.00045(15)	0.00085(16)	-0.00272(17)
Bi9	0.01169(17)	0.01281(19)	0.01743(19)	-0.00150(14)	0.00745(14)	0.00071(16)
Bi10	0.01173(17)	0.0164(2)	0.01725(19)	0.00271(15)	0.00597(15)	0.00060(17)
Bi11	0.0224(3)	0.0105(3)	0.0159(3)	-0.0028(2)	0.0071(2)	-0.0016(2)
Ca11	0.0224(3)	0.0105(3)	0.0159(3)	-0.0028(2)	0.0071(2)	-0.0016(2)
Bi12	0.0263(3)	0.0202(4)	0.0240(3)	-0.0047(2)	0.0137(3)	-0.0014(3)
Ca12	0.0263(3)	0.0202(4)	0.0240(3)	-0.0047(2)	0.0137(3)	-0.0014(3)
Bi13	0.0314(5)	0.0294(6)	0.0138(4)	-0.0081(4)	0.0049(4)	-0.0013(4)
Ca13	0.0314(5)	0.0294(6)	0.0138(4)	-0.0081(4)	0.0049(4)	-0.0013(4)
Bi14	0.0224(7)	0.0290(9)	0.0353(9)	0.0030(5)	0.0127(6)	0.0035(6)
Ca14	0.0224(7)	0.0290(9)	0.0353(9)	0.0030(5)	0.0127(6)	0.0035(6)
V1a	0.0139(4)	0.0105(4)	0.0127(4)	-0.0001(3)	0.0057(4)	-0.0003(3)
V1b	0.0110(7)	0.0101(3)	0.0084(4)	-0.0015(3)	0.0019(4)	0.0015(3)
V1c	0.0117(6)	0.0091(4)	0.0092(4)	-0.0024(4)	0.0027(4)	0.0006(3)
V1d	0.0119(4)	0.0086(4)	0.0123(7)	-0.0016(3)	0.0067(4)	-0.0008(4)
V1e	0.0122(5)	0.0096(4)	0.0103(7)	-0.0028(3)	0.0056(5)	-0.0011(4)

Table IV: Ea activation energies (eV) and σ conductivities (S.cm^{-1}) of $MBi_6V_2O_{15}$ (M=Pb, Sr, Ca, Cd, $Na_{0.5}Bi_{0.5}$).

$R(M^{2+})_{VI}$ coordinence	Material	σ (S.cm^{-1}) at 500°C	Ea (eV)	σ (S.cm^{-1}) at 800°C
1,18	$PbBi_6V_2O_{15}$	$3{,}36.10^{-6}$	1.19	$1{,}13.10^{-3}$
1,16	$SrBi_6V_2O_{15}$	$3{,}54.10^{-5}$	0.91	$1{,}78.10^{-3}$
1,00	$CaBi_6V_2O_{15}$	$2{,}28.10^{-6}$	1.17	$5{,}98.10^{-4}$
0.95	$CdBi_6V_2O_{15}$	$4{,}07.10^{-6}$	1.21	$1{,}15.10^{-3}$
1.02	$Na_{0.5}Bi_{6.5}V_2O_{15}$	$2.89.10^{-6}$	0.96	$2.103.10^{-3}$

Figure captions

Fig. 1- (010) projection of MBi$_6$V$_2$O$_{15}$ related structures (M=Pb, Sr, Ca, Cd, Na$_{0.5}$Bi$_{0.5}$): Ca based sample. Viewing of related fluorite cell (a), and VO$_4$ tetrahedrons (b).

Fig. 2- Evidence of VO$_4$ disordering in Ca based MBi$_6$V$_2$O$_{15}$ related sample.

Fig. 3- Dependence of the "mean cationic radius" versus Unit Cell volume, in the (Bi, M) mixed sites 11, 12, 13, 14 for MBi$_6$V$_2$O$_{15}$-type family.

Fig. 4- Conductivity Arrhenius plots of MBi$_6$V$_2$O$_{15}$ materials (M=Pb, Sr, Ca, Cd, Na$_{0.5}$Bi$_{0.5}$).

Fig. 5- MBi$_6$V$_2$O$_{15}$ related structure (M=Pb, Sr, Cd, Ca, Na$_{0.5}$Bi$_{0.5}$) viewed as cationic layers *(a)* or OBi$_4$, O(Bi, M)$_4$ and VO$_4$ tetrahedron layers arrangements *(b)*.

Fig. 6- MBi$_6$V$_2$O$_{15}$–type materials (M=Pb, Sr, Ca, Cd): Evolution of « slab+interslab » thickness (observed distorted lattice), and of theoretical cubic fluorite cell diagonal, versus r$_{VI}$ (M^{2+}).